Ultrathin epitaxial cobalt films on graphene for spintronic investigations and applications

2010 New J. Phys. 12 103040

(http://iopscience.iop.org/1367-2630/12/10/103040)

New Journal of Physics
The open-access journal for physics

Ultrathin epitaxial cobalt films on graphene for spintronic investigations and applications

Chi Vo-Van[1], Zoukaa Kassir-Bodon[1], Hongxin Yang[2], Johann Coraux[1,4], Jan Vogel[1], Stefania Pizzini[1], Pascale Bayle-Guillemaud[3], Mairbek Chshiev[2], Laurent Ranno[1], Valérie Guisset[1], Philippe David[1], Violaine Salvador[3] and Olivier Fruchart[1,4]

[1] Institut Néel, CNRS and Université Joseph Fourier, BP166, F-38042 Grenoble Cedex 9, France
[2] SPINTEC (UMR8191 CEA/CNRS/UJF/G-INP), CEA Grenoble, INAC, 38054 Grenoble Cedex 9, France
[3] CEA-Grenoble, INAC/SP2M/LEMMA, 17 rue des Martyrs, Grenoble, France
E-mail: johann.coraux@grenoble.cnrs.fr and olivier.fruchart@grenoble.cnrs.fr

New Journal of Physics **12** (2010) 103040 (15pp)
Received 28 July 2010
Published 26 October 2010
Online at http://www.njp.org/
doi:10.1088/1367-2630/12/10/103040

Abstract. Graphene is an attractive candidate in spintronics for a number of reasons, among which are its electric-field-controlled conductivity, its expected long spin lifetime and its two-dimensional nature. A number of recent proposals call for the development of high-quality ferromagnetic thin films in contact with graphene, whereas only thick polycrystalline or three-dimensional (nanoclusters) morphologies have been demonstrated so far. We report on the growth of flat, epitaxial ultrathin Co films on graphene using pulsed laser deposition. These display perpendicular magnetic anisotropy (PMA) in the thickness range 0.5–1 nm, in agreement with our first-principles calculations. PMA, epitaxy and ultra-small thickness bring new perspectives on graphene-based spintronic devices making use of the zero-field control of an arbitrary magnetization direction, band matching between electrodes and graphene, and interface phenomena such as the Rashba effect and electric field control of magnetism.

S Online supplementary data available from stacks.iop.org/NJP/12/103040/mmedia

[4] Authors to whom any correspondence should be addressed.

Contents

1. Introduction

The promising potential of graphene in spintronics, exceeding that of other carbon materials, has been highlighted in a wealth of theoretical predictions over the last few years. Similarly to carbon nanotubes, efficient spin transport and injection have been proposed, making use of the low spin–orbit and hyperfine interactions in carbon, combined with a high conductivity. But graphene brings this in two dimensions, which allows complex networks to be designed by lithography, and promises a better control of the interfaces with other materials to build hybrid architectures. However, spin transport reported so far [1] is much less efficient than in carbon nanotubes [2], possibly due to the strengthening of the spin–orbit interaction by extrinsic sources such as substrate-induced ripples [3] or adsorbed molecules [4]. Not only spin transport but also spin polarization in graphene is a topic of intense interest. For this, the two-dimensional (2D) nature of graphene is again appealing, either for shaping nanoribbons whose edges may intrinsically carry spin-polarized currents [5] or because extended contact to a suitable support is needed, inducing Rashba spin splitting of the conduction bands [6]–[8]. Graphene may also be inserted between two planar ferromagnets to build giant magnetoresistance junctions operated in a current perpendicular to the plane configuration, with neither too low (like for giant magnetoresistance) nor too high (like for tunnel magnetoresistance) resistance-area product, and with extremely thin spacers [9, 10].

The magnetoresistive effect outlined in the latter proposal calls for the availability of epitaxial ferromagnetic/graphene/ferromagnetic trilayers, due to the importance of band matching with graphene [11]. This requires that epitaxial graphene be prepared on ferromagnetic supports, which was demonstrated years ago [12], and also requires the development of epitaxial 2D ferromagnetic layers on top of graphene. We foresee that such layers may serve as building blocks in a number of spintronics setups beyond the scope of magnetoresistive junctions. We anticipate, for instance, that a large Rashba field may develop in an ultrathin 2D metallic ferromagnetic layer sandwiched between graphene and another metal layer of a heavy element such as gold, due to a strong out-of-plane electron potential gradient resulting from the structural inversion asymmetry imposed by the two distinct interfaces. This field may exceed that in Pt/Co/alumina trilayers where a strong s-d-mediated Rashba field was recently observed [13]. Also, contrary to relatively thick ferromagnetic substrates employed so far [7, 14], ultrathin films offer the opportunity to tune the spontaneous magnetization direction

as a function of the film thickness, from in-plane to perpendicular. Thus crossed spin-polarizers could be achieved.

To the best of our knowledge, there exists no report about truly 2D films of transition metals having a thickness ranging from one to a few atomic layers on either graphite or graphene. Molecular beam epitaxy (MBE) in ultrahigh vacuum (UHV) yields three-dimensional (3D) clusters [15] even when the deposition is carried out down to a few tens of kelvins. Indeed superstructures such as moirés on graphite [16] or graphene [17]–[22], or on the reconstructed graphitic layer of SiC [23, 24], may provide 2D lattices of nucleation sites for the clusters. In the absence of superstructures, cluster nucleation is sparse and proceeds at defect sites or at random when the clusters are large enough to become immobile. Large adatom and cluster diffusion lengths on graphene and graphite were calculated by first principles [25]–[27], consistent with sparse nucleation.

Here, instead of MBE, we use pulsed laser deposition (PLD), which as we will show allows us to prepare ultrathin 2D Co films. We developed these films on graphene/Ir(111)/Al_2O_3(0001). Iridium was chosen as a supporting surface, because graphene growth atop Ir is self-limited to a single layer [28] and because Ir only weakly perturbs the electronic properties of graphene [29]. Thus, the features of overgrowth of Co and its magnetic properties are expected to be largely applicable to isolated graphene. In view of spintronics setups for which lithography and transport measurements should be carried out, we employed novel high-quality Ir(111) thin films developed by us instead of bulky single crystals, which are costly and would shunt the current. Cobalt was finally capped with Au to protect the films from air oxidation for *ex situ* characterizations. The Co films display perpendicular magnetic anisotropy (PMA) in the thickness range 0.5–1 nm. First-principles calculations reveal an active role of the Co/graphene interface in the magnetism of Co, which allows us to sustain PMA. Good uniformity of the layers is confirmed by the very low coercivity (2–10 mT) over the entire PMA range, suitable for the reliable control of magnetization via magnetic or electric fields.

The paper is organized as follows. Experimental setups and methods are described in the first section. We then present the growth and structural characterization of the Co films. We finally proceed with the analysis of the magnetic properties.

2. Experiments and methods

The synthesis was conducted in a UHV setup that is described elsewhere [30]. The base pressure was 3×10^{-11} and 2×10^{-10} Torr in the chambers for metal and graphene growth, respectively. Temperatures were measured with a pyrometer. C-plane sapphire (Al_2O_3(0001)) 2-inch-wafers (Roditi Ltd) were used as substrates[5]. These were cut with either a focused laser or a diamond saw to fit them in Omicron sample holders. Sample cleaning followed the procedure described in [30] and surface preparation of sapphire was completed by double outgassing at 850 °C under UHV during 45 min. The metallic layers (Ir, Co and Au) were grown by PLD with 10 pulses per second, each pulse with a fluence in the range 0.1–1 J cm^{-2}, yielding an evaporation rate of the order of 0.5 Å min^{-1}. A computer-controlled mask was moved in front of the sample for producing wedge-shaped Co layers (figure 1). Graphene was grown by catalytic thermal decomposition of ethene (C_2H_4) [28]. The gas was brought

[5] Sapphire substrates with a miscut angle of 0.25° and 0.03°. We found no effect of the miscut angle on the growth or magnetism.

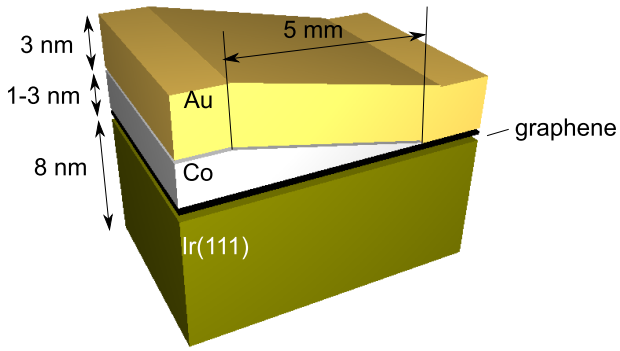

Figure 1. Schematics of a Co wedge deposit on graphene/Ir(111), capped by a Au layer. Typical thicknesses for the various layers are displayed.

in the vicinity of the sample surface by a dosing tube of 10 mm diameter, ending 10 mm away from the sample surface, which ensured a local partial pressure higher than in the rest of the chamber.

Scanning tunneling microscopy (STM; Omicron) and reflection high-energy electron diffraction (RHEED; Riber; 10 kV) were performed *in situ* at room temperature. Cross-section high-resolution transmission electron microscopy (HR-TEM) was conducted *ex situ* using a JEOL 4000EX setup with an acceleration voltage of 400 kV and a point resolution of 0.17 nm. Cross-section specimens were obtained by mechanical grinding for thinning and ion milling using a precision ion polishing system.

Magnetization reversal was probed by the magneto-optical Kerr effect (MOKE). With a first setup, we gathered hysteresis loops, using a laser (wavelength 633 nm) illuminating the surface over a few microns wide spot. The incidence of the laser is 30° away from the surface normal, in which case MOKE is essentially sensitive to perpendicular magnetization (polar MOKE). The incident beam is linearly polarized. The reflected beam is split with a Wollaston prism to compute a difference signal, which is proportional to the magnetic moment of the sample perpendicular to the plane. The magnetic field was applied perpendicular to the surface. The hysteresis loops were averaged over hundreds to thousands of cycles performed at 11 Hz. MOKE microscopy was conducted in a commercial microscope (Evico-magnetics). The images are recorded by a CCD camera and can be averaged. The initial image corresponding to the saturated magnetization was subtracted from all images. Extraordinary Hall effect (EHE) measurements were carried out at 300 K and up to 6 T using the four-probe configuration. Mechanical as well as Ag-paint contacts were used on the non-patterned (i.e. as-grown) samples.

For first-principles calculations, we used the Vienna *ab initio* simulation package (VASP) [31] with the generalized gradient approximation (Perdew–Burke–Ernzerhof) [32] and projector augmented wave potentials [33]. The calculations were performed in two steps. First, out-of-plane structural relaxation was allowed and the Kohn–Sham equations solved with no spin–orbit interaction taken into account for determining the most favourable adsorption geometry of graphene on Co. Then the spin–orbit coupling was included and the total energy of the system was determined as a function of the orientation of the magnetic moments. The k-point mesh used in all calculations is $15 \times 15 \times 1$. The energy cutoff was set to 520 eV. The atomic structures are relaxed until the forces are smaller than 0.001 eV Å^{-1}. For the anisotropy calculations, the total energies are converged to 10^{-7} eV.

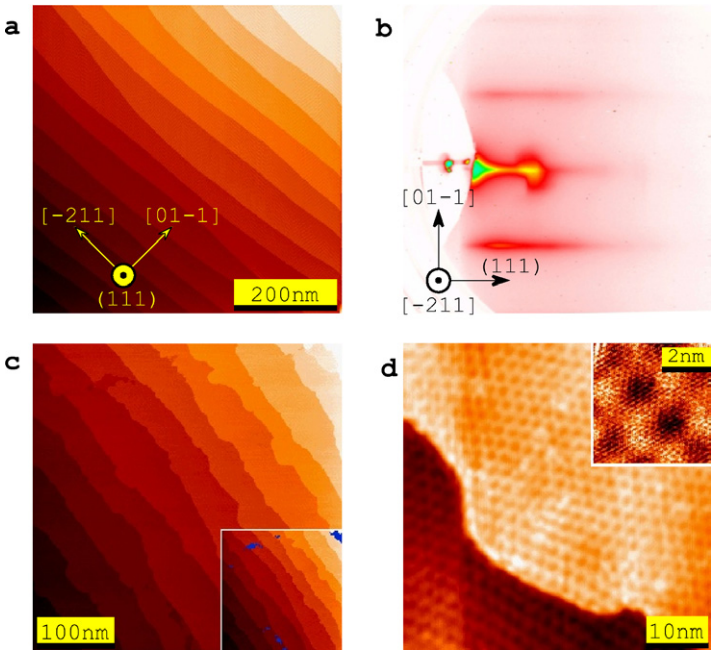

Figure 2. (a) $600 \times 600\,\mathrm{nm}^2$ STM topograph of a 8-nm-thick Ir(111) buffer layer epitaxially grown on sapphire C. The contrast highlights atomic terraces, whose $\simeq 60\,\mathrm{nm}$ width is directly related to the miscut angle of the wafer, here 0.25°. (b) RHEED pattern of an Ir surface such as shown in (a), revealing the single-crystalline quality of Ir. The beam azimuth is of type ⟨112⟩, while the diffusion vector probed here is of type ⟨110⟩. (c) $400 \times 400\,\mathrm{nm}^2$ STM topograph of a single sheet of graphene epitaxially grown on an Ir buffer layer such as shown in (a). The few remaining areas not covered by graphene are highlighted in blue in the inset. (d) $50 \times 50\,\mathrm{nm}^2$ STM topograph of graphene. The triangular superstructure with 2.5 nm periodicity is a moiré pattern, resulting from the lattice misfit between the Ir(111) and graphene [40]. The $5 \times 5\,\mathrm{nm}^2$ inset reveals the atomic resolution of the moiré.

3. Preparation of 2D ultrathin cobalt films on graphene

We recently developed the growth of high-quality thin Ir(111) films on C-plane sapphire [34]. The STM topograph of an 8-nm-thick film grown at 430 °C and annealed at 850 °C for 30 min reveals atomically smooth terraces (figure 2(a)) whose width is limited only by the miscut of the sapphire wafer. The RHEED pattern shown in figure 2(b) is typical of a high-quality single-crystalline surface [34]. The growth of graphene at 800 °C under 1×10^{-8} torr ethene pressure (the local pressure, at the sample surface, is higher) for 10 min proceeds similarly to the growth on single crystals [28]. Graphene coverage approaches 100% (figure 2(c)) and a typical graphene/Ir(111) moiré is observed (figure 2(d)). The in-plane epitaxial relationship is sapphire$[11\bar{2}0]$ ∥ Ir$[\bar{2}11]$ ∥ graphene$[1\bar{1}00]$ ∥ Co$[\bar{2}11]$ as determined by RHEED and/or *ex situ* x-ray diffraction for sapphire and the metal layers. We found no evidence of the rotational variants reported by Loginova *et al* [35]. Graphene replicates the atomic smoothness of the Ir(111) buffer layer by extending coherently across its atomic steps. The uniformity

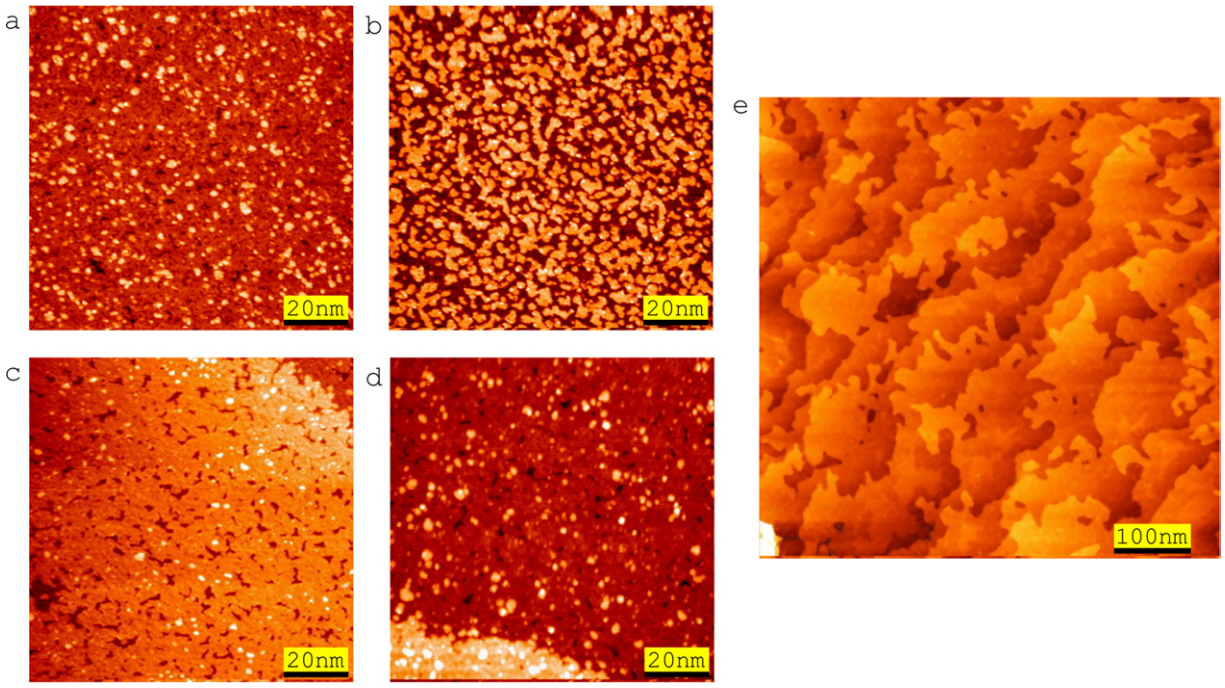

Figure 3. (a–d) $100 \times 100\,\mathrm{nm}^2$ STM topographs of Co deposited at room temperature on graphene/Ir(111). The sequence illustrates close to perfect layer-by-layer growth for Co, for 3 (a), 3.4 (b), 4 (c) and 5 (d) atomic layers. (e) A $600 \times 600\,\mathrm{nm}^2$ STM topograph of a Co film of thickness 1.7 nm ($\simeq 9$ atomic layers) annealed at 450 °C. The topography is similar for other thicknesses.

of graphene, which reflects that of the Ir(111) surface, surpasses that in other supported systems where polycrystalline thin films are employed and/or multilayer graphene cannot be avoided [36]–[39].

The PLD growth at room temperature of Co on the graphene sheet proceeds nearly perfectly layer-by-layer up to about 1.5 nm (figures 3(a)–(d)). Only monolayer-high islands and/or trenches are found, arising from the unavoidable non-integer mean number of atomic layers found at an arbitrary stage of deposition. The growth mode is noticeably different from that with MBE, which leads to metal clusters at the same temperature and in this range of thicknesses [41]. We believe that the higher instantaneous deposition rate of PLD leads to higher nucleation density of smaller clusters in the initial stages of the growth and that this tends to force layer-by-layer growth [42, 43]. For thicknesses larger than 1.5 nm deviations from the layer-by-layer mode set in and roughness progressively increases, probably due to the progressive increase of mean island size. For both regimes, the annealing of the deposit at 450 °C yields a flat Co film, with a mean terrace width again only limited by the miscut angle of the wafer (figures 3(a)–(d)).

Prior to *ex situ* HR-TEM observations and magnetic characterizations the Co film is capped with a 3-nm-thick Au deposit at room temperature. HR-TEM (figure 4(a)) confirms the smoothness and uniformity of the Co layer. The Co layer contains stacking faults (figure 4(b)) and can therefore be viewed as a mixture of hexagonal compact (hcp) Co (its stable structure in

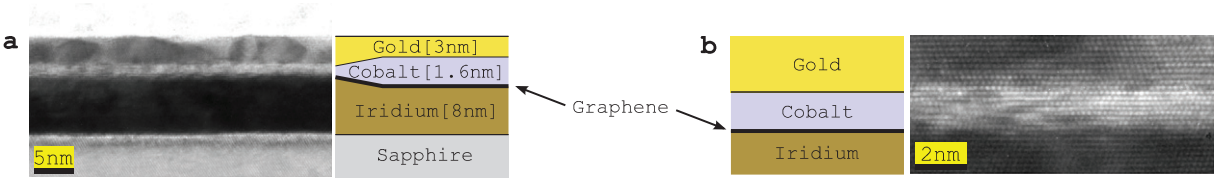

Figure 4. (a) Large and (b) close-up cross-sectional HR-TEM images of a 1.6 nm Co film capped with Au on graphene/Ir(111). In (b), stacking faults are observed in the Co atomic lattice and a mixture of face-centered cubic and hcp regions is seen.

the bulk form at room temperature) and face-centered cubic (fcc) Co (stable above 422 °C in the bulk, but often stabilized in nanostructures). The graphene sheet cannot be clearly identified on these images, probably due to the graphene–Co spacing being similar to that of Co [11].

4. Magnetic properties

4.1. Magnetic anisotropy

Let us first discuss the magnetic anisotropy energy (MAE) of these films, which determines the easy axis of magnetization. In a uniaxial system, the density of MAE can be described to first order as $E = K \sin^2\theta$ with K in units of J m^{-3}. Here θ is the direction of magnetization with respect to the normal to the layers. Positive values of K mean PMA, while negative values mean alignment of magnetization in the plane of the layers. Hysteresis loops provide evidence for PMA in the range of thickness $t \in [0.5\text{–}1]$ nm (figure 7(a)). In this range, the remanence is complete, i.e. the magnetization remains fully perpendicular to the film plane after the external field has been set back to zero. Let us recall that for most magnetic films the magnetization is strongly constrained to lie in-the-plane, due to the negative contribution to the MAE of the magnetostatic energy $E_{\text{Shape}} = -\mu_0 M_S^2/2$, which would arise in the case of perpendicular magnetization. An effective PMA may be achieved only for selected cases where the magnetostatic energy is overcome by positive contributions to the MAE. Here we leave aside those cases where positive contributions arise from bulk magnetocrystalline anisotropy such as for intermetallics 4f–3d, FePt, CoPt, etc, because we focus on ultrathin films to highlight interfacial effects with graphene. In ultrathin films, positive contributions to the MAE may arise from interface and/or magneto-elastic effects. As both terms decay typically like $1/t$, PMA is restricted to thicknesses typically below 1–3 nm. Known ultrathin stackings with PMA are either all metal based [44] or more recently metal oxide based [45, 46].

The magnetic field needed to saturate the magnetization of a system along a hard direction is a measure of the strength of its MAE. In the simple case of uniaxial second-order anisotropy, which we assumed here, the field required is the so-called anisotropy field $H_a = 2K/\mu_0 M_S$, which we have measured at 300 K using EHE, for a Co thickness of 0.7 nm. The field has been applied in the plane of the heterostructure. Due to experimental misalignment in the cryostat, a small out-of-plane angle of the order of a few degrees exists between the magnetic field and the sample surface. This misalignment is large enough to break the symmetry and allows for nonzero net perpendicular remanence, i.e. nonzero EHE at zero applied field. The 80 ± 10 mT coercive field (see figure 5) is consistent with the already measured out-of-plane 3 mT coercive

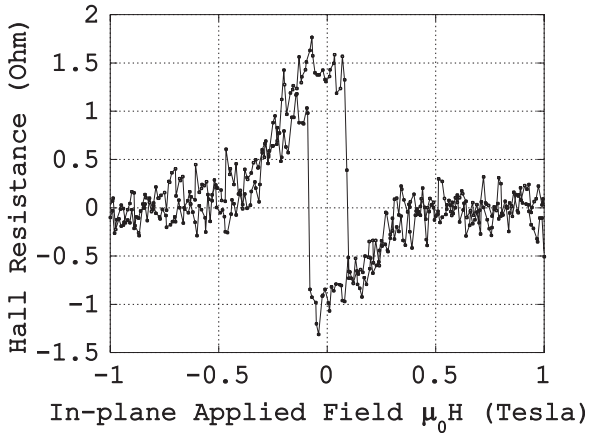

Figure 5. Hall resistance as a function of the applied field, at 300 K. The direction of the applied field is almost in the plane of the sample, within an uncertainty of a few degrees.

field, assuming a misalignment angle of 2°. The magnitude of the experimental EHE is 1.4 mΩ at 300 K. Note that this value is low due to the fact that most of the current flows in the metallic bottom and capping layers[6]. A saturation field is clearly evidenced (see figure 5), from whose fit an anisotropy field of 0.37 ± 0.05 T is deduced, corresponding to an MAE of 264 ± 36 kJ m^{-3}, i.e. $+0.185 \pm 0.025$ mJ m^{-2} for the 0.7-nm-thick Co layer.

Let us discuss these results in view of the literature. As already mentioned, in ultrathin films, the anisotropy differs from bulk values owing to several effects such as interfacial anisotropy, magneto-elasticity and quantum confinement. While the latter two are difficult to estimate and/or control, trends in interfacial anisotropy were largely investigated by substitutions of interfacial elements. This leads to series of figures depending on the couple of elements [44, 47]. Large-spin–orbit elements such as Pt, Au and Pd favour perpendicular anisotropy, particularly for the case of Co layers. Thus Au/Co/Au films display perpendicular magnetization with full remanence up to ≈ 1.7 nm. The anisotropy field is of the order of 2 T around a thickness of 1 nm [48], while the Co/Au interfacial anisotropy is evaluated to ≈ 0.5 mJ m^{-2} [49].

Comparing these values concerning symmetric Au/Co/Au films with our Au/Co/graphene system, it is clear, from the lower values that we obtained for both anisotropy field and critical

[6] Due to the metallic character of the bottom layer (Ir + graphene) and capping layer (Au), most of the in-plane current does not flow through the Co layer. The square resistance of a 9-nm-thick Ir layer is 5.9 Ω sq^{-1} with a residual resistivity ratio of 8.8 (measurements not shown here). Assuming 80 and 10 Ω sq^{-1} specific resistances for the Co and Au regions, respectively, and that the specific resistance of graphene should drop by at least one order of magnitude as compared to undoped graphene (1000 Ω sq^{-1}) due to charge transfer from Ir [29] and Co [11], less than 10% of the current should flow through Co if the heterostructure behaves as resistors in parallel (i.e. neglecting interface contributions and the finite-thickness effect). The literature values for Co EHE (0.24×10^{-8} Ω cm T^{-1}) and magnetization (1.43×10^{6} A m^{-1}) yield an EHE resistance of 62 mΩ for 0.7 nm thickness. The measured EHE of 1.4 mΩ corresponds to 2.4% of the current flowing through Co, indeed less than 10%. Other effects may contribute foward further decreasing the EHE (<100% out-of-plane remanence, partial short circuit of the transverse EHE electric field by the metallic layers).

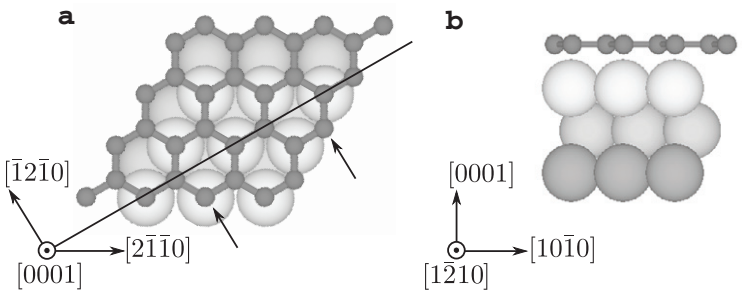

Figure 6. Geometry of the relaxed Co/graphene slab derived from the first-principles calculations. (a) Top view and (b) cross-sectional view in the plane defined by [0001] and [$10\bar{1}0$], as depicted with a line and arrows in (a). Co (hcp) and carbon appear in light and dark gray. Crystallographic indexes refer to the Co lattice.

upper thickness for perpendicular anisotropy, that the major effect for sustaining perpendicular anisotropy should arise from the (upper) Au/Co interface. Let us evaluate this quantitatively.

In the following, we expressed all anisotropies as densities normalized to the thickness of the considered film, 0.7 nm, so that they read as J m^{-2}.

In a crude approach for estimating the Co/graphene interface anisotropy, we assume that the MAE of the Co layer can be separated into contributions from Co/Au and Co/graphene interfaces, magnetocrystalline and shape anisotropies for Co. For the latter two, we consider the bulk values for hcp Co at room temperature [50]. This neglects effects of finite temperature, which however are enhanced in low dimensions, as we shall discuss later on. The bulk magnetocrystalline anisotropy equals +0.36 mJ m^{-2} for 0.7 nm thickness. The volume density for the shape anisotropy, $-\mu_0 M_S^2/2$, corresponds to -0.82 mJ m^{-2} for 0.7 nm thickness assuming bulk magnetization. Based on the expected Co/Au interface anisotropy of +0.5 mJ m^{-2}, one then derives +0.15 mJ m^{-2} for the Co/graphene interface to reach the overall value of 0.185 mJ m^{-2} derived from EHE. Interestingly, assuming the usual $1/t$ variation of MAE would yield 0.98 nm thickness for the vanishing of PMA, in very good agreement with the experimental result (1 nm). At this stage, we conclude that a Co/graphene interface seems to favour perpendicular anisotropy, although to a lesser extent than an Au/Co interface.

We used first-principles calculations to try to further highlight the role of the Co/graphene interface in PMA. As MAE depends subtly on strain and local environment, the structural details of the Co slab and its interfaces should be taken into account accurately for a quantitative discussion. However, whereas Co and graphene have very similar lattice parameters, a large in-plane lattice mismatch exists between bulk Au and Co ($\simeq$14%) and Ir and Co/graphene ($\simeq$7%). Co/graphene, Au and Ir lattices are therefore *a priori* not commensurate and could only be approximated with a unit cell of at least 10 nm lateral size, which is out of the reach of first-principles calculations. We therefore selected two simple cases that we compared: two slabs with a thickness of three atomic layers of Co, either free standing or in contact with a commensurate graphene sheet on one side (figure 6). Hexagonal compact Co, observed in (at least) a noticeable fraction of the films by TEM, was considered. A 2 nm vacuum slab was added on each side with periodic boundary conditions. Note that experimentally the graphene/Ir(111) interface is expected to have little influence since the interaction (charge transfer and orbital hybridization) between graphene and Ir(111) is limited [29]. As the most stable structural

arrangement for graphene on Co(0001) (2.507 Å in-plane lattice parameter) we found that half the carbon atoms sit right atop the Co atoms of the uppermost layer, and the other half of the carbon atoms sit in an fcc site (figure 6), consistent with recent theoretical results [10]. The interface distance is 0.211 nm after out-of-plane relaxation.

A comprehensive first-principles exploration of the system is beyond the scope of this paper and will be reported elsewhere. We present two findings that are of particular relevance in view of the observed PMA. A significant hybridization of graphene π orbitals with Co 3d ones was predicted by first-principles calculations [11]. We find that this affects the magnitude of the Co magnetic moments at the graphene interface. While the total magnetic moment of Co in the middle layer (1.633 μ_B) is close to the bulk one, the moment at the interface with graphene is reduced by 0.1 μ_B. In contrast, we find an increase of 0.1 μ_B at the free surface of Co, which is consistent with the usual situation where magnetic moments are enhanced at interfaces with vacuum, most transition metals or oxides, and explained on the basis of the narrowing of the 3d band of the ferromagnet [51, 52]. Looking at the significant effect of graphene on the magnetism of Co, it is clear that the MAE should be affected.

The MAE of the slabs was computed as the difference in total energy values for in-plane and out-of-plane magnetic moments. The three-atomic-layer-thick Co slabs, with and without a graphene overlayer, both exhibit PMA, with magnitude +1.0133 and +1.2274 mJ m^{-2}, respectively, excluding the magnetostatic energy. This means that, again based on the sole discussion of the contribution of interfaces, both the Co/vacuum and Co/graphene interfaces promote PMA, the former, however, slightly more than the latter. This agrees with the EHE measurements.

Let us discuss our theoretical findings in the context of existing works. Our calculations suggest that Co/vacuum favours perpendicular magnetization. This is consistent with other recent first-principles calculations [53], but is in contradiction with earlier reports based on tight binding [54] and *ab initio* [55] calculations or experimental studies [44, 56]. These contradictions probably stem from the oversimplified model separating MAE in contributions for the bulk and interfaces, the latter with a universal well-defined value depending solely on the interfacial elements. Layer-resolved first-principles calculations point to complex variations of MAE as a function of the thicknesses of the magnetic film [55, 57] and capping layers [53]. El Gabaly *et al* [53] highlight that anisotropy at interfaces indeed arises not only from the capping layer but also from the surface and sub-surface magnetic atomic layers. These authors stress that below four atomic layers the concept of interface anisotropy should fail, much beyond the approximation made above about the value of magnetization in layers of finite thickness (combined thermal and low-dimensional effects). Differences with all-metal interfaces are also expected due to the large magneto-elastic contribution to the MAE [53] arising from the large misfit with elements such as Au and Pt, which does not occur with graphene. Further experiments with varying interfaces and thicknesses in a systematic way are required for shedding light on these issues.

4.2. Magnetization reversal

We now discuss magnetization reversal features. The coercive field $\mu_0 H_C$ is of the order of a few mT (figures 7(a) and (b)). This value is several orders of magnitude lower than the anisotropy field (0.37 T). This suggests [58] that magnetization reversal proceeds by the nucleation of a few reversed domains at defects of the extended film (sample edges, scratches, etc),

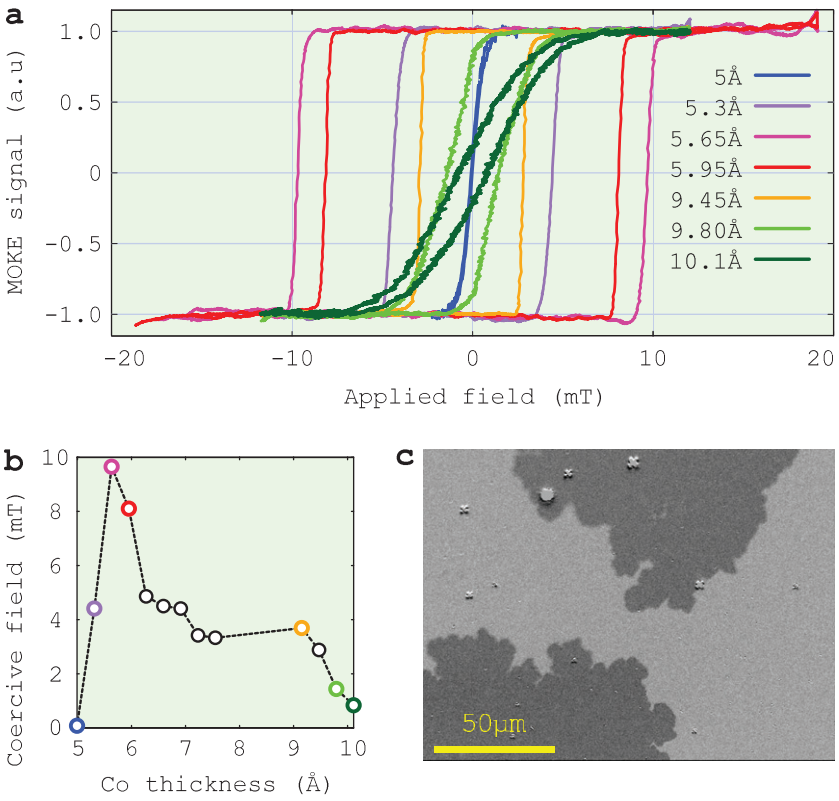

Figure 7. (a) Focused MOKE hysteresis loops of Co (capped with 3 nm Au, on graphene/Ir(111)) with various thicknesses in the range of PMA. The loops have been cycled and averaged at 11 Hz. (b) Coercive field (H_C) as a function of the thickness of the Co layer, as derived from loops in (a) (and others which are not displayed for clarity in (a)). The peak of coercivity at low thickness may be related either to the expected variation of anisotropy, roughly inversely proportional to the thickness, or to the relative influence of thickness fluctuations. (c) $170 \times 130\,\mu m^2$ MOKE microscopy image of a 0.8 nm Co film (capped with 3 nm Au, on graphene/Ir(111)) following partial magnetization reversal with a field of 3.5 mT applied perpendicular to the plane of the film, opposite to the initial magnetization direction. The initial domain appears bright, while the reversed domains appear dark. The latter nucleated outside the field of view, and inflated through thermally activated domain wall propagation, a so-called creep regime (see text). A complete movie of a magnetization reversal process is provided as supplementary material, available at stacks.iop.org/NJP/12/103040/mmedia.

followed by an easy propagation of domain walls through the remaining part of the film. This picture of very weak pinning is further suggested by the abruptness of magnetization reversal around H_C. A confirmation of this fact is gained by monitoring magnetic domains during magnetization reversal, using Kerr microscopy. Under quasi-static conditions, the average size of the domains is indeed larger than 100 μm (figure 7(c)), and magnetization reversal proceeds solely through the propagation of domain walls (see also the movie provided as supplementary material, available from stacks.iop.org/NJP/12/103040/mmedia). The domain wall propagation

is stochastic and occurs in sudden jumps; it is thermally activated. This is the so-called creep regime, characteristic of weak pinning [59]. Low coercivity is difficult to achieve in PMA materials because their MAE is large by nature. Thus all local variations and defects are liable to induce energy barriers and energy wells proportional to this MAE and thus of large magnitude. Similar weak pinning and low coercivity have been demonstrated in a couple of selected metal-on-metal systems, in the very special cases where magnetism is weakened by either selecting extremely low thickness [60] or by weakening anisotropy and magnetism by ion irradiation [61]. For Co/graphene low coercivity is maintained through the entire range of thickness for PMA, which points to the intrinsic quality of the layer microstructure.

5. Conclusion

We developed ultrathin, atomically smooth Co films on graphene, using PLD growth. PLD was crucial for its ability to favour layer-by-layer growth. As a graphene support for this growth, we selected ultrasmooth epitaxial graphene prepared on nanometer-thick Ir(111) films on sapphire wafers, a system mimicking isolated graphene due to the weak graphene–Ir interaction and well suited to device realization. The Co films were capped with Au and exhibit PMA in the thickness range of 0.5–1 nm, resulting in spontaneous perpendicular magnetization. EHE measurements and first-principles calculations show that hybridization at the Co/graphene interface promotes PMA, with a contribution of the same order of magnitude as the Co/Au interface. Based on the measurement of PMA, first-principles calculations and comparison with the literature, PMA was mainly ascribed to the Au/Co interface, with a weaker contribution from the Co/graphene interface. PMA ensures that a high magnetic remanence, low magnetostatic interactions with the surrounding due to the ultrathin aspect ratio of the layers and high thermal stability can be achieved, even for nanostructures down to a very small lateral size, which is promising for sustaining high-remanence nanomagnets in devices down to very small lateral dimensions.

PMA also opens the door to the easy realization of graphene-based devices with cross-magnetized electrodes such as those needed for efficient spin-transfer torque magnetization precession. Other graphene-relevant interfacial effects expected in such asymmetric layers pertain to novel ways of controlling magnetization, such as Rashba fields [13] and electric fields [62].

We suggest that instead of graphene/Ir(111), other graphene supports may be employed. Exfoliated graphene, graphene/SiC and graphene prepared on metals and transferred to insulating supports [36, 37] would *a priori* be well suited to lateral transport devices.

Acknowledgments

We thank J Debray for wafer orientation. CVV, HY and MC acknowledge financial support from Fondation Nanosciences. This work was partially supported by ANR-07-NANO-034 Dynawall.

Reference

[1] Tombros N, Jozsa C, Popinciuc M, Jonkman H T and van Wees B J 2007 Electronic spin transport and spin precession in single graphene layers at room temperature *Nature* **448** 571

[2] Hueso L E, Pruneda J M, Ferrari V, Burnell G, Valdés-Herrera J P, Simons B D, Littlewood P B, Artacho E, Fert A and Mathur N D 2007 Transformation of spin information into large electrical signals using carbon nanotubes *Nature* **445** 410

[3] Ishigami M, Chen J H, Cullen W G, Fuhrer M S and Williams E D 2007 Atomic structure of graphene on SiO_2 *Nano Lett.* **7** 1643–8
[4] Moser J, Verdaguer A, Jiménez D, Barreiro A and Bachtold A 2008 The environment of graphene probed by electrostatic force microscopy *Appl. Phys. Lett.* **92** 123507
[5] Son Y W, Cohen M L and Louie S G 2006 Half-metallic graphene nanoribbons *Nature* **444** 347–9
[6] Varykhalov A, Sánchez-Barriga J, Shikin A M, Biswas C, Vescovo E, Rybkin A, Marchenko D and Rader O 2008 Electronic and magnetic properties of quasifreestanding graphene on Ni *Phys. Rev. Lett.* **101** 157601
[7] Rader O, Varykhalov A, Sánchez-Barriga J, Marchenko D, Rybkin A and Shikin A M 2009 Is there a Rashba effect in graphene on 3d ferromagnets? *Phys. Rev. Lett.* **102** 57602
[8] Gierz I, Dil J H, Meier F, Slomski B, Osterwalder J, Henk J, Winkler R, Ast C R and Kern K 2010 Giant anisotropic spin splitting in epitaxial graphene arXiv:1004.1573
[9] Karpan V M, Giovannetti G, Khomyakov P A, Talanana M, Starikov A A, Zwierzycki M, van den Brink J, Brocks G and Kelly P J 2007 Graphite and graphene as perfect spin filters *Phys. Rev. Lett.* **99** 176602
[10] Yazyev O V and Pasquarello A 2009 Magnetoresistive junctions based on epitaxial graphene and hexagonal boron nitride *Phys. Rev.* B **80** 35408
[11] Giovannetti G, Khomyakov P A, Brocks G, Karpan V M, van den Brink J and Kelly P J 2008 Doping graphene with metal contacts *Phys. Rev. Lett.* **101** 026803
[12] Oshima C and Nagashima A 1997 Ultra-thin epitaxial films of graphite and hexagonal boron nitride on solid surfaces *J. Phys.: Condens. Matter* **9** 1–20
[13] Miron I M, Gaudin G, Auffret S, Rodmacq B, Schuhl A, Pizzini S, Vogel J and Gambardella P 2010 Current-driven spin torque induced by the Rashba effect in a ferromagnetic metal layer *Nature Mater.* **9** 230–4
[14] Weser M, Rehder Y, Horn K, Sicot M, Fonin M, Preobrajenski A B, Voloshina E N, Goering E and Dedkov Yu S 2010 Induced magnetism of carbon atoms at the graphene/Ni(111) interface *Appl. Phys. Lett.* **96** 012504
[15] Binns C, Baker S H, Demangeat C and Parlebas J C 1999 Growth, electronic, magnetic and spectroscopic properties of transition metals on graphite *Surf. Sci. Rep.* **34** 107–70
[16] Xhie J, Sattler K, Ge M and Venkateswaran N 1993 Giant and supergiant lattices on graphite *Phys. Rev.* B **47** 15835–41
[17] N'Diaye A T, Bleikamp S, Feibelman P J and Michely T 2006 Two-dimensional Ir cluster lattice on a graphene moire on Ir(111) *Phys. Rev. Lett.* **97** 215501
[18] N'Diaye A T, Gerber T, Busse M, Myslivecek J, Coraux J and Michely T 2009 A versatile fabrication method for cluster superlattices *New J. Phys.* **11** 103045
[19] Donner K and Jakob P 2009 Structural properties and site specific interactions of Pt with the graphene/Ru (0001) moiré overlayer *J. Chem. Phys.* **131** 164701
[20] Pan Y, Gao M, Huang L, Liu F and Gao H J 2009 Directed self-assembly of monodispersed platinum nanoclusters on graphene moiré template *Appl. Phys. Lett.* **95** 093106
[21] Zhang H, Fu Q, Cui Y, Tan D L and Bao X H 2009 Fabrication of metal nanoclusters on graphene grown on Ru(0001) *Chin. Sci. Bull.* **54** 2446–50
[22] Sicot M, Bouvron S, Zander O, Rüdiger U, Dedkov Y S and Fonin M 2010 Nucleation and growth of nickel nanoclusters on graphene moiré on Rh (111) *Appl. Phys. Lett.* **96** 093115
[23] Chen W, Loh K P, Xu H and Wee A T S 2004 Growth of monodispersed cobalt nanoparticles on 6H–SiC (0001) honeycomb template *Appl. Phys. Lett.* **84** 281
[24] Poon S W, Chen W, Tok E S and Wee A T S 2008 Probing epitaxial growth of graphene on silicon carbide by metal decoration *Appl. Phys. Lett.* **92** 104102
[25] Jensen P, Blase X and Ordejón P 2004 First principles study of gold adsorption and diffusion on graphite *Surf. Sci.* **564** 173–8
[26] Lehtinen P O, Foster A S, Ayuela A, Krasheninnikov A, Nordlund K and Nieminen R M 2003 Magnetic properties and diffusion of adatoms on a graphene sheet *Phys. Rev. Lett.* **91** 17202
[27] Chan K T, Neaton J B and Cohen M L 2008 First-principles study of metal adatom adsorption on graphene *Phys. Rev.* B **77** 235430

[28] Coraux J, N'Diaye A T, Engler M, Busse C, Wall D, Buckanie N, Meyer zu Heringdorf F-J, van Gastel R, Poelsema B and Michely T 2009 Growth of graphene on Ir(111) *New J. Phys.* **11** 023006
[29] Pletikosic I, Kralj M, Pervan P, Brako R, Coraux J, N'Diaye A T, Busse C and Michely T 2009 Dirac cones and minigaps for graphene on Ir(111) *Phys. Rev. Lett* **102** 056808
[30] Fruchart O, Eleoui M, Jubert P O, David Ph, Santonacci V, Cheynis F, Borca B, Hasegawa M and Meyer C 2007 Growth modes of Fe(110) revisited: a contribution of self-assembly to magnetic materials *J. Phys.: Condens. Matter* **19** 053001
[31] Kresse G and Furthmüller J 1996 Efficient iterative schemes for *ab initio* total-energy calculations using a plane-wave basis set *Phys. Rev.* B **54** 11169
[32] Perdew J P, Burke K and Ernzerhof M 1996 Generalized gradient approximation made simple *Phys. Rev. Lett.* **77** 3865
[33] Blöchl P E 1994 Projector augmented-wave method *Phys. Rev.* B **50** 17953
[34] Vo-Van C *et al* 2010 to be published
[35] Loginova E, Nie S, Thürmer K, Bartelt N C and McCarty K F 2009 Defects of graphene on Ir(111): rotational domains and ridges *Phys. Rev.* B **80** 085430
[36] Reina A, Jia X, Ho J, Nezich D, Son H, Bulovic V, Dresselhaus M S and Kong J 2009 Large area, few-layer graphene films on arbitrary substrates by chemical vapor deposition *Nano Lett.* **9** 30
[37] Kim K S, Zhao Y, Jang H, Lee S Y, Kim J M, Kim K S, Ahn J-H, Kim P, Choi J-Y and Hong B H 2009 Large-scale pattern growth of graphene films for stretchable transparent electrodes *Nature* **457** 706
[38] Li X *et al* 2009 Large-area synthesis of high-quality and uniform graphene films on copper foils *Science* **324** 1312
[39] Sutter E, Albrecht P and Sutter P 2009 Graphene growth on polycrystalline Ru thin films *Appl. Phys. Lett.* **95** 3109
[40] Coraux J, N'Diaye A T, Busse C and Michely T 2008 Structural coherency of graphene on Ir(111) *Nano Lett.* **8** 565
[41] Michely T 2010 private communication
[42] Shen J, Gaib Z and Kirschner J 2004 Growth and magnetism of metallic thin films and multilayers by pulsed-laser deposition *Surf. Sci. Rep.* **52** 163
[43] Clavero C, Cebollada A, Armelles G and Fruchart O 2010 Growth mode, magnetic and magneto-optical properties of pulsed-laser-deposited Au/Co/Au(111) trilayers *J. Magn. Magn. Mater.* **322** 651
[44] Johnson M T, Bloemen P J H, den Broeder F J A and de Vries J J 1996 Magnetic anisotropy in metallic multilayers *Rep. Prog. Phys.* **59** 1409–58
[45] Rodmacq B, Manchon A, Ducruet C, Auffret S and Dieny B 2009 Influence of thermal annealing on the perpendicular magnetic anisotropy of Pt/Co/AlO_x trilayers *Phys. Rev.* B **79** 024423
[46] Ikeda S, Miura K, Yamamoto H, Mizunuma K, Gan H D, Endo M, Kanai S, Hayakawa J, Matsukura F and Ohno H 2010 A perpendicular-anisotropy CoFeBMgO magnetic tunnel junction *Nature Mater.* **9** 721
[47] Gradmann U 1993 Magnetism in ultrathin transition metal films *Handbook of Magnetic Materials* vol 7 (Amsterdam: Elsevier) p 1
[48] Chappert C, Dang K L, Beauvillain P, Hurdequint H and Renard D 1986 Ferromagnetic resonance studies of very thin cobalt films on a gold substrate *Phys. Rev.* B **34** 3192
[49] Beauvillain P, Boounouh A, Chappert C, Mégy R, Ould-Mahfoud S, Renard J P, Veillet P, Weller D and Corno J 1994 Effect of submonolayer coverage on magnetic anisotropy of ultrathin cobalt film M/Co/Au(111) with M = Au, Cu, Pd *J. Appl. Phys.* **76**
[50] Wohlfarth E P 1988 Iron, cobalt and nickel *Handbook of Magnetic Materials* vol 1 ed K H J Buschow (Amsterdam: North-Holland) pp 1–70
[51] Freeman A J and Ru quian Wu 1991 Electronic structure theory of surface, interface and thin-film magnetism *J. Magn. Magn. Mater.* **100** 497
[52] Calandra C, Chiarotti G, Gradmann U, Jacobi K, Manghi F, Maradudin A A, Tong S Y and Wallis R F 1994 *Physics of Solid Surfaces: Electronic and Vibrational Properties (Landolt–Börstein New Series Group III* vol 24b) ed G Chiariotti (Heidelberg: Springer)

[53] El Gabaly F, McCarty K F, Schmid A K, de la Figuera J, Carmen Muñoz M, Szunyogh L, Weinberger P and Gallego S 2008 Noble metal capping effects on the spin-reorientation transitions of Co/Ru(0001) *New J. Phys.* **10** 073024

[54] Bruno P 1989 Tight-binding approach to the orbital magnetic moment and magnetocrystalline anisotropy of transition-metal monolayers *Phys. Rev.* B **39** 865

[55] Dorantes-Dávila J, Dreyssé H and Pastor G 2003 Magnetic anisotropy of transition-metal interfaces from a local perspective: reorientation transitions and spin-canted phases in Pd capped Co films on Pd(111) *Phys. Rev. Lett.* **91** 197206

[56] Rusponi S, Cren T, Weiss N, Epple M, Claude L, Buluschek P and Brune H 2003 The remarkable difference between surface and step atoms in the magnetic anisotropy of 2d nanostructures *Nature Mater.* **2** 546

[57] Yang H *et al* 2010 to be published

[58] Givord D, Rossignol M and Barthem V M T S 2003 The physics of coercivity *J. Magn. Magn. Mater.* **258–259** 1

[59] Ferré J 2001 Dynamics of the magnetization reversal: from continuous to patterned ferromagnetic films *Spin Dynamics in Confined Magnetic Structures* ed K Ounadjela (Heidelberg: Springer) pp 127–68

[60] Lee J-C, Kim K-J, Ryu J, Moon K-W, Yun S-J, Gim G-H, Lee K-S, Shin K-H, Lee H-W and Choe S-B 2010 Universality between current- and field-driven domain wall dynamics in ferromagnetic nanowires arXiv:0912.5127v1

[61] Chappert C, Barnas H, Ferr J, Kottler V, Jamet J-P, Chen Y, Cambril E, Devolder T, Rousseaux F, Mathet V and Launois H 1998 Planar patterned magnetic media obtained by ion irradiation *Science* **280** 1919

[62] Weisheit M, Fähler S, Marty A, Souche Y, Poinsignon Ch and Givord D 2007 Electric field-induced modification of magnetism in thin-film ferromagnets *Science* **315** 349